

SCIENTIFIC REPORTS

OPEN

Hybrid Photonic Cavity with Metal-Organic Framework Coatings for the Ultra-Sensitive Detection of Volatile Organic Compounds with High Immunity to Humidity

Received: 19 October 2016
Accepted: 22 December 2016
Published: 31 January 2017

Jifang Tao^{1,*}, Xuerui Wang^{2,*}, Tao Sun¹, Hong Cai¹, Yuxiang Wang², Tong Lin², Dongliang Fu¹, Lennon Lee Yao Ting¹, Yuandong Gu¹ & Dan Zhao²

Detection of volatile organic compounds (VOCs) at parts-per-billion (ppb) level is one of the most challenging tasks for miniature gas sensors because of the high requirement on sensitivity and the possible interference from moisture. Herein, for the first time, we present a novel platform based on a hybrid photonic cavity with metal-organic framework (MOF) coatings for VOCs detection. We have fabricated a compact gas sensor with detection limitation ranging from 29 to 99 ppb for various VOCs including styrene, toluene, benzene, propylene and methanol. Compared to the photonic cavity without coating, the MOF-coated solution exhibits a sensitivity enhancement factor up to 1000. The present results have demonstrated great potential of MOF-coated photonic resonators in miniaturized gas sensing applications.

Volatile organic compounds (VOCs), such as xylene, benzene, and formaldehyde, are those chemicals with high vapor pressures at room temperature. They exist extensively in our daily life and may cause health problems including cancer, headaches, central nervous system damage, *etc.*^{1–7}. It is therefore of great importance to develop sensitive and reliable detection technologies for VOCs to monitor their health hazard. Besides health issues, VOCs detection is also essential in several other applications such as food safety⁸, cosmetic industry⁹, and diagnosis of diseases as biomarkers through breath analysis¹⁰. Currently, gas-phase VOCs detection is mainly conducted by gas chromatograph (GC) or mass spectrometer (MS), whose bulky size and high cost limit their wider applications^{11,12}. Some other compact gas-phase VOCs sensors based on nanocantilevers¹³, graphane^{14,15} or carbon nano-tubes^{16,17} were demonstrated with very high sensitivity and fast response, but their sensitivity drifts seriously in long time running and they are unstable to be used in real test conditions due to strong cross-response to humidity¹⁸. Another alternative technology for VOCs sensing is absorption spectroscopy, which measures the optical power variation in photon-gas interaction and have unique advantages such as low cross-response, fast response and high accuracy^{19,20}. However, the absorption spectra of VOCs normally cover a broad range from ultraviolet to middle infrared, and the absorption coefficients are relative weak^{21–24}. It is very difficult to realize ppb-level detection. Up to now, to build a universal optical sensing platform for VOCs detection is still quite challenging.

Photonic micro-ring resonator (MRR) is a powerful detection and analysis tool that has vast applications in biomedical research^{25,26}, environmental monitoring²⁷ and pharmaceuticals²⁸. In a MRR, the light propagates in the form of circulating waveguide modes (CWMs) coming from total internal reflection of the curved boundary between the high and low refractive index (RI) medium²⁹. The CWMs generate evanescent fields at outside of the MRR and respond to changes in the dielectric properties³⁰ of the surroundings. To quantify the sensing

¹Institute of Microelectronics, A*STAR (Agency for Science, Technology and Research), 2 Fusionopolis Way, #08-02 Innovis Tower, 138634, Singapore. ²Department of Chemical & Biomolecular Engineering, National University of Singapore, 4 Engineering Drive 4, 117585, Singapore. *These authors contributed equally to this work. Correspondence and requests for materials should be addressed to Y.G. (email: guyd@ime.a-star.edu.sg) or D.Z. (email: chezhao@nus.edu.sg)

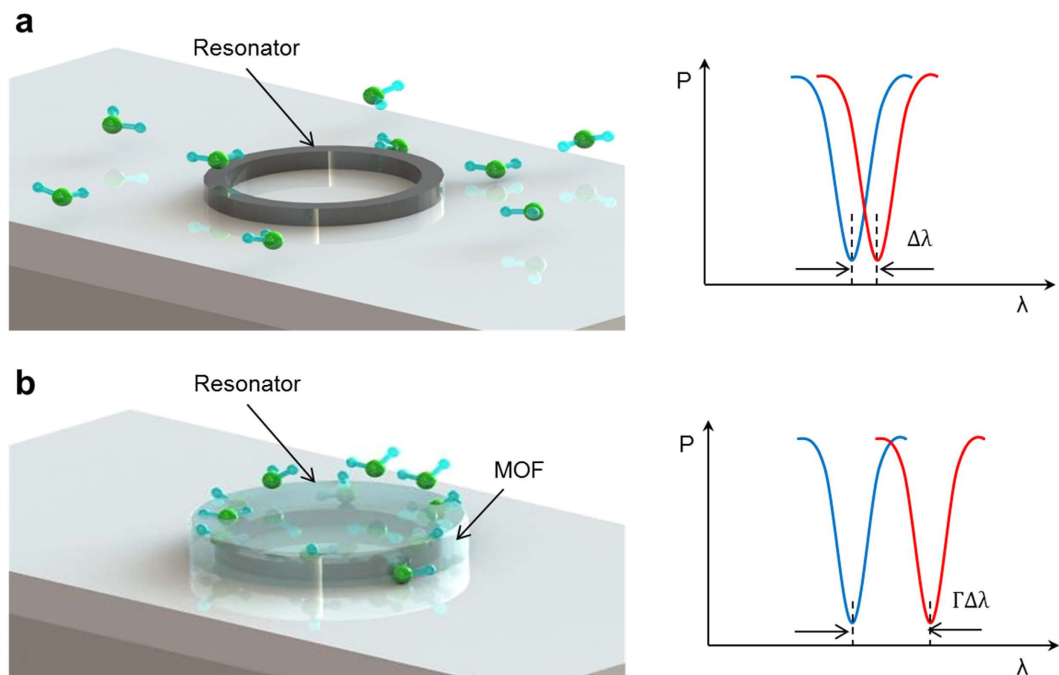


Figure 1. Schematic representation the gas sensing by use of an optical micro-ring resonator. Blue line and red line in spectrum show resonant wavelengths without/with gas. Gas molecules surrounding the micro-ring resonator changes its complex dielectric function, which causes a resonance shift of the micro-ring resonator that can be detected. (a) Gas sensing with a normal micro-ring resonator without coating. Spectra are almost overlapped with a barely detectable change ($\Delta\lambda$). (b) Gas sensing with the hybrid photonic-MOF device. The spectrum shift induced by gas absorption can be identified clearly ($\Gamma\Delta\lambda$).

capability, the detection limit (DL) with a unit of refractive index unit (RIU) is used (typically in the range of 10^{-7} – 10^{-5}), which is the ratio of the resonance shift of the resonator to the local refractive index of the medium. DL can be improved by increasing the light-matter interactions, such as to pre-concentrate analytes onto resonators³¹. Currently, most of the reported materials used for pre-concentration are polymers, such as polyimide and polydimethylsiloxane²⁹. They are easy to form coating layers but are limited by long-term stability and poor gas adsorption capability. Metal-organic frameworks (MOFs) are emerging porous materials composed of organic ligands and inorganic metal clusters^{32–36}. They have the unique advantages of large specific surface areas and mechanical stability close to that of crystalline semiconductors⁴⁰. Moreover, their growth and patterning by standard semiconductor fabrication processes have been demonstrated recently^{36–39}. Herein, we report the fabrication of MRR coated with MOF layers serving as pre-concentrating materials for enhanced detection sensitivity toward gas-phase VOCs.

Design and Fabrication

This design fully utilizes the strong absorption properties of MOFs^{40–42} and the ultra-high quality factor (Q-factor) of photonic resonator structures to demonstrate an on-chip VOCs sensing approach with an enhancement of detection factor as high as 10^3 compared with non-coated ones. Figure 1 illustrates the working mechanism of our approach. The resonant spectra of micro-ring are labeled as blue (blank) and red (under test), respectively. The micro-ring alone causes a barely detectable change ($\Delta\lambda$) upon gas exposure because of the limited amount of gas molecules nearby (Fig. 1a). In contrast, dramatically increased amount of gas molecules can be adsorbed by the MOF coating of the waveguides, leading to an obvious resonance shift ($\Gamma\Delta\lambda$) of the micro-ring that can be easily detected with increased detection sensitivity (Fig. 1b).

We selected ZIF-8 as the external MOF coating material because of its high surface area ($1840\text{ m}^2\text{ g}^{-1}$), good water stability, and high light transmittance in NIR^{43,44}. ZIF-8 has large cavities (11.6 \AA) and small apertures (3.4 \AA) that can be expressed as a space-filling packing of regular truncated octahedral, as shown in Fig. 2b. The VOCs molecule can penetrate and are adsorbed within ZIF-8 cavities. The device fabrication processes are shown in Fig. 2a. Silicon nitride (Si_3N_4) waveguide was used to fabricate the MRR. It has a radius of $40\text{ }\mu\text{m}$, and the coupling gap between the bus waveguide and the MRR is around 300 nm . A 23,000 Q-factor is obtained in the testing. Compared with silicon waveguides, Si_3N_4 waveguides has a low refractive index that allows a smaller confinement factor inducing a larger evanescent optical field, which results in a strong interaction between the incident light and gas molecules. Fabrication started with a $3.5\text{ }\mu\text{m}$ thick silicon dioxide (SiO_2) layer and a 400 nm thick Si_3N_4 layer deposition in a low-pressure chemical vapour deposition (LPCVD) furnace. Followed by waveguide structures defined using deep UV photolithography, reactive ion etching (RIE) was used to transfer waveguide patterns onto the Si_3N_4 layer. After that, a 200 nm thick SiO_2 cladding layer was blanket deposited on the entire device by plasma-enhanced chemical vapour deposition (PECVD) to reduce the waveguide transmission loss and protect

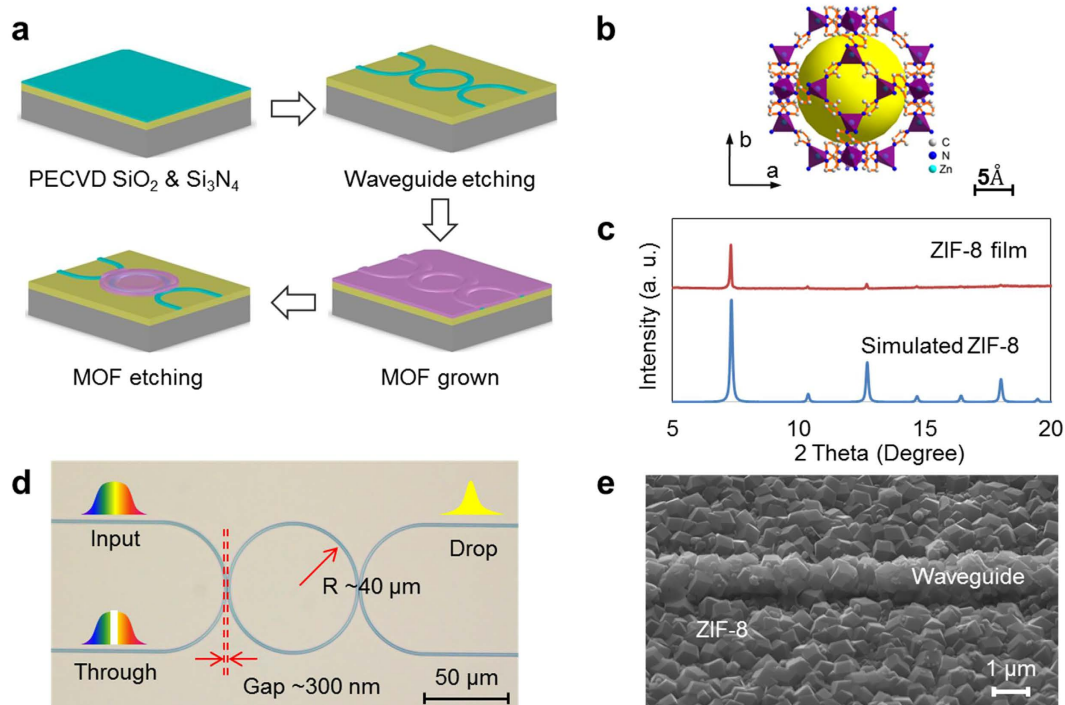


Figure 2. (a) Illustration of the fabrication process flow for hybrid photonic-MOF sensor device. (b) Chemical structure of the ZIF-8 nanocrystals. (c) X-ray diffraction pattern. (d) Micrograph of the hybrid photonic-MOF gas sensor. The micro-ring resonator is coupled with two bus waveguides that have two integrated inversed-tip couplers for input and output of optical signals from and to optical fibers. (e) Scanning electron microscope image of the top view.

the Si_3N_4 waveguides. Then, the photonic device was washed in sulfuric acid before ZIF-8 growth. Layer-by-layer intergrowth process was employed for the synthesis of ZIF-8 coating, whose structure can be confirmed by the powder X-ray diffraction patterns (Fig. 2c). Finally, ZIF-8 thin film was patterned using lithography and etched by sulfuric acid (Fig. 2d). The MRR is side coupled with two bus waveguides to readout the drop and through signals. The morphology of the ZIF-8 coating was inspected by scanning electron microscopes (SEM) as shown in Fig. 2e. The bus waveguides and MRR has a dimension of $1\ \mu\text{m} \times 0.4\ \mu\text{m}$, and the thickness of the ZIF-8 coating is around $1\ \mu\text{m}$. To activate the ZIF-8 film, the device was immersed in anhydrous methanol for 3 days with frequently refreshing of methanol to remove the unreacted zinc ions and 2-methylimidazole. After the removal of methanol, the film was dried under a dynamic vacuum at $120\ ^\circ\text{C}$ for 12 h.

Experimental Results

To evaluate the performance of the ZIF-8 film on gas adsorption, a gas adsorption experiment has been carried out by use of surface area and porosimetry system (Model: Micromeritics ASAP 2020). Figure 3a shows nitrogen (N_2) sorption isotherm at 77 K, which exhibits a typical type I isotherm pattern indicating the microporous nature of ZIF-8. The hysteresis loop at high relative pressure shows the existence of mesopores in addition to the microporous network⁴⁵. ZIF-8 is a well-known material with high hydrophobicity adsorbing limited amount of moisture at ambient condition⁴⁶. Compared with the negligible uptake of water vapour, Fig. 3b shows that ZIF-8 possesses an S-shaped isotherm for methanol uptake demonstrating the framework affinity to methanol. Moreover, the trapped methanol molecules could reversibly escape from the cavities of ZIF-8 (yellow color area in Fig. 2b). The reversible and marginal water uptake endows ZIF-8 the merits of high immunity to humidity, and hence preserve the ZIF-8 based sensor from moisture attack, while cross-responding to humidity is regarded as one of most challenges for gas sensors. Moreover, it is possible to trap gases with large molecule size, e.g. toluene. This phenomenon should be largely attributed to the exothermal adsorption of toluene molecules ($5.25\ \text{\AA}$) from the relative small aperture of ZIF-8 ($3.4\ \text{\AA}$).

To measure the response of the photonic-MOF sensor in the presence of VOCs vapours, we utilized a gas mixing system and controlled the concentration by two mass flow controllers (MFCs) to control the carrier gas (N_2) and the VOCs flow as shown in Fig. 4a. The gas flows were maintained at 100 sccm during the whole experiments. A T-shape glass gas cell was used to control the gas environment atop the chip that was affixed by a UV-glue. The species and pressure of the gas above the chip were governed by the flexible tubing connected to the glass cell. A photograph of the gas cell attached to a chip is shown in Fig. 4b. The chip was mounted on a vertical alignment system for light coupling between fibers and chip. The input light was from a tunable laser light source (ANDO AQ4321D) while the output light was received by an embedded power meter synchronized with the tunable laser

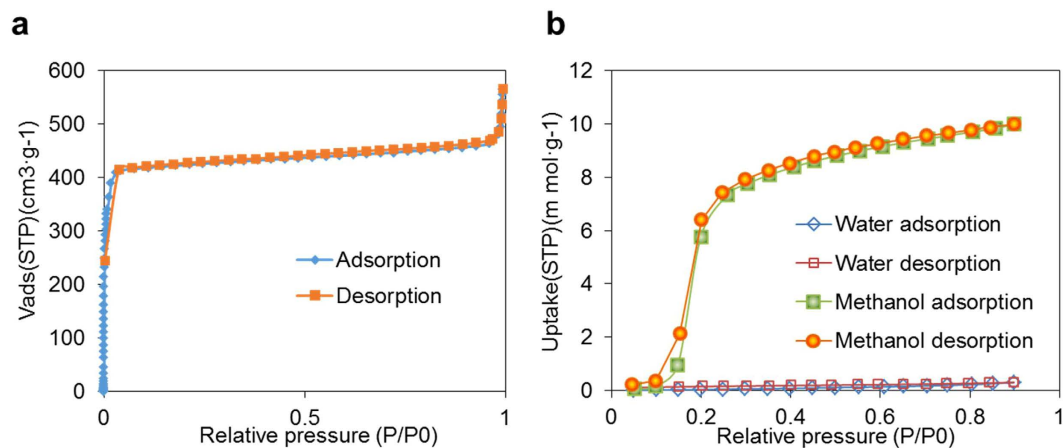


Figure 3. (a) N_2 sorption isotherms at 77 K of ZIF-8. (b) Absorption isotherms of water and methanol by ZIF-8 that dedicates the merits of high immunity to humidity, while cross-responding to humidity is regarded as one of most challenges for gas sensors.

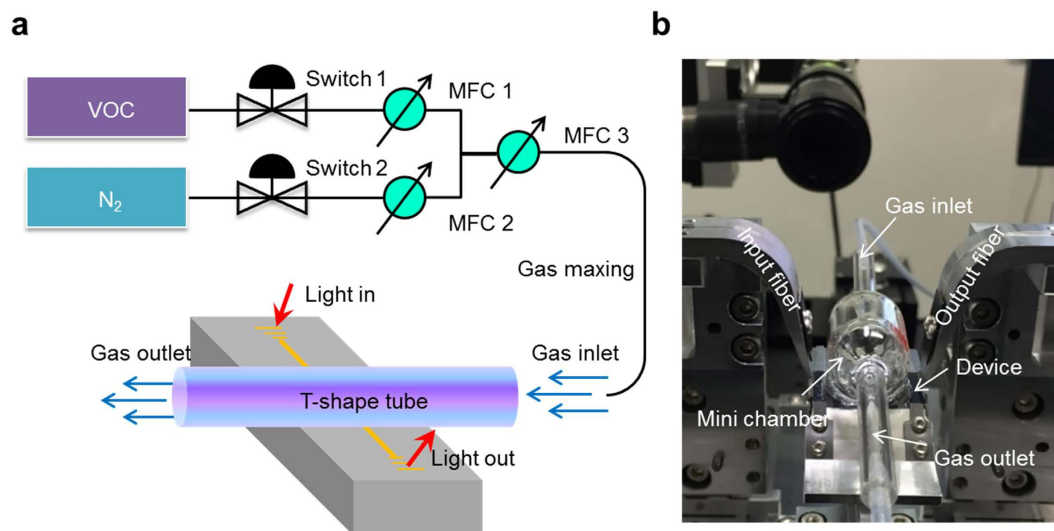


Figure 4. (a) Experimental apparatus using a gas mixture system and optical alignment system. (b) Illustration of the device sitting on the three-axis alignment system covered by a gas cell.

source. Both the input and output signals were transmitted to a computer for real-time monitoring; the transmission spectra were plotted subsequently.

The optical properties of the device were simulated and characterized. The optical fields of the MRR decaying exponentially outside its geometric boundaries were simulated by finite element method (FEM, Fig. 5a). The evanescent field, which has energy accounting for 5% of the total photonic energy, can sense the changes of ZIF-8's RI effectively. In this simulation, we assume the dispersion of ZIF-8 at near infrared region is zero because of the small portion of the total light in ZIF-8 film⁴⁷. The effective index generated by FEM also can be used to estimate the RI of ZIF-8 through calculating the free spectral range (FSR) of the MRR. From the FSR, we can identify the RI of the ZIF-8 and effective index of waveguide, as pointed by "A" as shown in Fig. 5b. Our calculation based on the thin layer of ZIF-8 with a thickness of 1 μm . Transmission spectra of the MRR were measured with (red line) and without (blue line) ZIF-8, as shown in Fig. 5c. The FSR of the MRR increasing from 4.65 nm to 4.76 nm was observed when 1- μm thick ZIF-8 was grown. The loaded Q-factor of the MRR was reduced from 23,000 to 14,000, as shown in the zoomed in view. The drop of the Q-factor induced by the growth of the ZIF-8 film was measured. It slightly increases the DL in the sensing due to the broaden 3-dB bandwidth. Based on the theoretical calculation of MRR, we can conclude that the ZIF-8 film has a refractive index of 1.38. This refractive index is on the lower end of the range of previously reported values, implying our film was more porous or had larger pores.

As mentioned above, the resonant wavelength of the MRR is strongly dependent on the changes of ZIF-8 RI induced by gas adsorption. The wavelength shifts monitored at around 1575.67 nm are shown in Fig. 6a. Five VOC vapours: methanol, propylene, benzene, toluene, and styrene, were injected separately into the device with a fixed concentration of 100 ppm carried by N_2 gas flows. The resonant wavelength exhibited a blueshift firstly, and

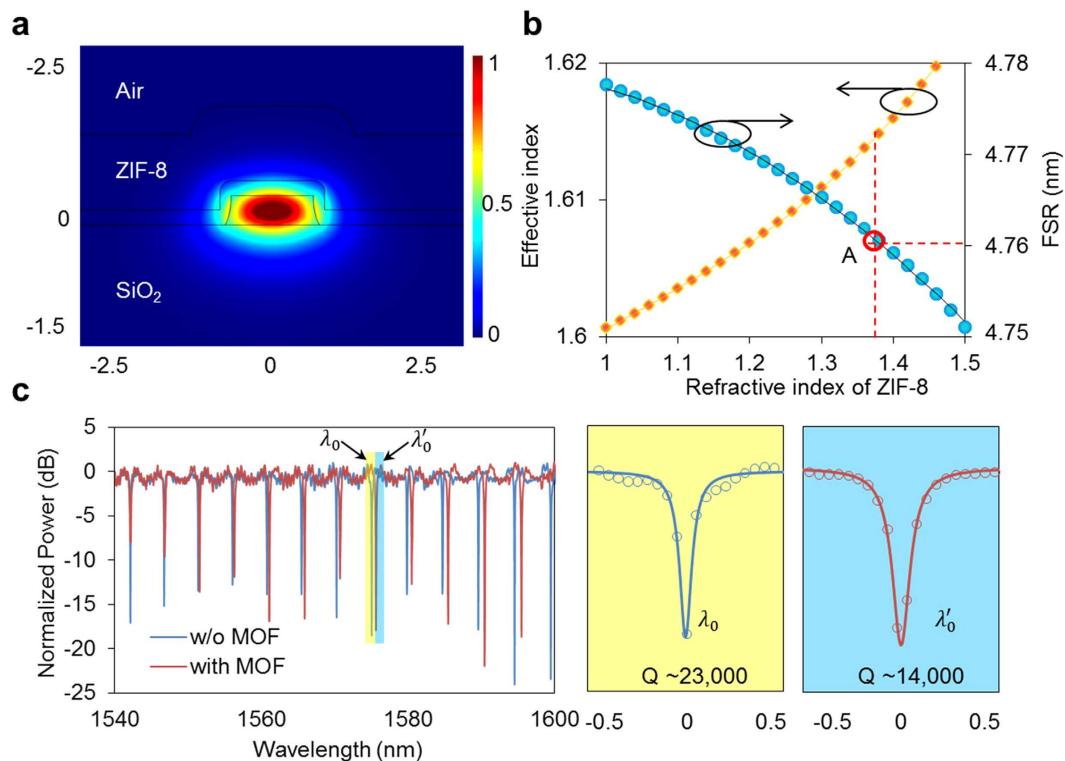


Figure 5. (a) Finite element method simulation results of the electrical component of the optical fields of the waveguide evanescently propagated in the hybrid photonic-MOF waveguide. (b) Theoretical calculation of the relationship between the refractive index of ZIF-8, effective index and FSR. (c) Transmission spectra measurements for resonator without MOF and with 1 μm thick MOF, and zoomed in view of the resonant dip.

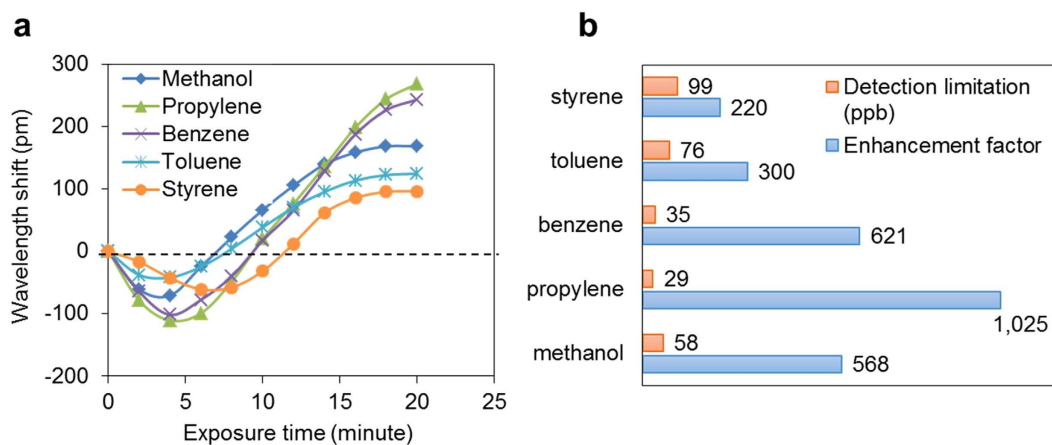


Figure 6. (a) Optical response of the hybrid photonic-MOF device to 20 minutes exposure of different VOCs with a fixed concentration of 100 ppm. (b) Enhancement factor and detection limitation of five VOCs at equilibrium.

then started to redshift for each gas, as shown in Fig. 6a. The blueshift happening at the initial stage is probably induced by air-cooling of the airflow and the heat exchange in the gas absorption. The redshift results from the increase in RI of ZIF-8 due to adsorption, which can offset the decrease of RI from the thermo-optic effect that can be well modelled with Fick's equation of diffusion^{48,49}. The equilibrium during the exposure time is between 30 to 45 minutes for these five VOC vapours, and the final shifts of the resonance are 172 pm, 341 pm, 282 pm, 131 pm, and 101 pm for methanol, propylene, benzene, toluene, and styrene, respectively. The long-time taken is attributed to the relative thick of the ZIF-8 film, as well as the unpassivated walls of the gas inlet tubing. In further studies, the long equilibrium time can be shortened by adopting thinner ZIF-8 films and advanced sensor packaging.

Solution	VOCs	Detection limitation	Response time	Reference
Microresonators with (poly) isobutylene coatings	Benzene	5.3 ppm	Not mentioned	53
	Toluene	1.2 ppm		
	<i>m</i> -Xylene	0.6 ppm		
Porous Co ₃ O ₄ concave nanocubes	Ethanol	10 ppm	<10 s	54
	Acetone			
	Toluene			
Hybrid photonic-MOF structure	Methanol	58 ppb	~30 minutes (depend on the MOF thickness)	This work
	Propylene	29 ppb		
	Benzene	35 ppb		
	Toluene	76 ppb		
	Styrene	99 ppb		

Table 1. Compare of VOCs detection based on miniature sensor.

The sensitivity of the sensor can be defined as wavelength shift ($\Delta\lambda$) over gas concentration (C), ($\Delta\lambda/C$). The wavelength shift ($\Delta\lambda$) is determined by the refractive index changes variation ($n - n_0$) with gas concentrations, which is expressed by initial resonant wavelength (λ_0), the magnitude of evanescent field (t), and initial group index (n_g).

$$\Delta\lambda = \lambda_0 t \frac{(n - n_0)}{n_g} \quad (1)$$

The refractive index of a gas mixture from the Lorenz-Lorentz equation is given by the relation⁵⁰

$$\frac{n^2 - 1}{n^2 + 2} = \sum_i R_i \rho_i \quad (2)$$

in which R_i and ρ_i are the specific refraction and the partial density of the i -type gas of the mixture, respectively. For 100-ppm VOCs mixture, the refractive index difference is as low as 10^{-7} RIU. It generates ~0.5 pm wavelength shifts at the best case if there is no pre-concentration, which is much smaller than the sensor with MOF coatings. Comparing to a MRR without pre-concentration/absorption layers, the hybrid photonic-MOF devices can improve the sensitivity up to 568, 1025, 621, 300, and 220 times for methanol, propylene, benzene, toluene, and styrene, respectively, as shown in Fig. 6b. Except the refractive index responding to different gases, the sensing performance also strongly relies on the uptake of VOCs molecule by ZIF-8 crystals⁵¹. For example, the low selectivity of styrene can be attributed to the fact that the styrene molecule (5.8 Å) is too bulky to penetrate into the cage of ZIF-8 because of the relative small aperture size of ZIF-8. As the resonant wavelength variation induced by the environmental temperature variation and tunable laser instability is around ± 0.1 pm in the experiments as previous mentioned⁵², the detection limits for these five VOC vapours are determined in the range from 29 to 99 ppb as shown in Fig. 6b. It is worth of noting that a more advanced temperature stabilization scheme and a higher accuracy wavelength tracker can be used for further improvement of detection accuracy.

The benchmark of the miniature MOF sensors is shown in Table 1. Based on the literature survey, there are three main solutions for gas detection by use of MOFs adsorption: (1) Mass weighting by use of coating MOFs onto Micro-electro-mechanical system (MEMS) resonators, in which the resonant frequency of the MEMS resonators changes as gas concentration⁵³; (2) Electrical sensing via measuring electrical characters, e.g. resistivity and conductivity. When MOFs expose in different gas species or different gas concentration, MOFs' electrical characters can be changed accordingly⁵⁴; (3) Measuring optical properties of MOFs, for example the refractive index of MOFs changes as gases species and concentrations. As shown in the Table 1, the detection limitation of the 3rd approach reported by this paper can be reduced further compared with weighting approaches and electrical sensing approaches. For the response time, it is strongly depended on the layer thickness of the MOF as discussed in previous section. Although the response time of 30 minutes is relative longer, it still can be adopted at some applications that require high-accuracy detection, such as indoor-air quality monitoring.

Conclusions

The paper demonstrates the proof-of-concept of a versatile and highly integrated sensing platform for VOCs detection by utilizing appropriate MOF coatings to achieve selective functionalization. The CMOS-compatible photonic resonator is employed to determine the concentration of VOCs on-chip with a detection limitation of ppb-level. The presented platform can also be used as a flexible tool to deeply explore the optical properties of MOFs. Our results open an avenue towards the highly sensitive gas detection using MOF-coated devices.

References

- Baek, S.-O., Kim, Y.-S. & Perry, R. Indoor air quality in homes, offices and restaurants in Korean urban areas-indoor/outdoor relationships. *Atmospheric Environment* **31**, 529–544 (1997).
- Daisey, J. M., Angell, W. J. & Apte, M. G. Indoor air quality, ventilation and health symptoms in schools: An analysis of existing information. *Indoor air* **13**, 53–64 (2003).

3. Wolkoff, P. Volatile organic compounds sources, measurements, emissions, and the impact on indoor air quality. *Indoor air* **5**, 5–73 (1995).
4. Jones, A. P. Indoor air quality and health. *Atmospheric Environment* **33**, 4535–4564 (1999).
5. Yu, C. & Crump, D. A review of the emission of VOCs from polymeric materials used in buildings. *Building and Environment* **33**, 357–374 (1998).
6. Wilkinson, P. *et al.* Public health benefits of strategies to reduce greenhouse-gas emissions: Household energy. *The Lancet* **374**, 1917–1929 (2009).
7. Hassan, M., Joshi, A., Madhavan, S. & Amonkar, M. Obesity and health-related quality of life: A cross-sectional analysis of the US population. *International journal of obesity* **27**, 1227–1232 (2003).
8. Khot, L. R., Panigrahi, S. & Lin, D. Development and evaluation of piezoelectric-polymer thin film sensors for low concentration detection of volatile organic compounds related to food safety applications. *Sensors and Actuators B: Chemical* **153**, 1–10 (2011).
9. Wheals, A. E., Basso, L. C., Alves, D. M. & Amorim, H. V. Fuel ethanol after 25 years. *Trends in Biotechnology* **17**, 482–487 (1999).
10. Peng, G. *et al.* Diagnosing lung cancer in exhaled breath using gold nanoparticles. *Nature Nanotechnology* **4**, 669–673 (2009).
11. Miekisch, W., Schubert, J. K. & Noeldge-Schomburg, G. F. Diagnostic potential of breath analysis-focus on volatile organic compounds. *Clinica Chimica Acta* **347**, 25–39 (2004).
12. Holmes, E., Wilson, I. D. & Nicholson, J. K. Metabolic phenotyping in health and disease. *Cell* **134**, 714–717 (2008).
13. Lavrik, N. V., Sepaniak, M. J. & Datskos, P. G. Cantilever transducers as a platform for chemical and biological sensors. *Review of Scientific Instruments* **75**, 2229–2253 (2004).
14. Deng, S. *et al.* Reduced graphene oxide conjugated Cu₂O nanowire mesocrystals for high-performance NO₂ gas sensor. *Journal of the American Chemical Society* **134**, 4905–4917 (2012).
15. Yavari, F. *et al.* High sensitivity gas detection using a macroscopic three-dimensional graphene foam network. *Scientific reports* **1** (2011).
16. Kong, X. Y., Ding, Y. & Wang, Z. L. Metal-semiconductor Zn-ZnO core-shell nanobelts and nanotubes. *The Journal of Physical Chemistry B* **108**, 570–574 (2004).
17. Modi, A., Koratkar, N., Lass, E., Wei, B. & Ajayan, P. M. Miniaturized gas ionization sensors using carbon nanotubes. *Nature* **424**, 171–174 (2003).
18. Washburn, A. L., Luchansky, M. S., Bowman, A. L. & Bailey, R. C. Quantitative, label-free detection of five protein biomarkers using multiplexed arrays of silicon photonic microring resonators. *Analytical Chemistry* **82**, 69–72 (2009).
19. Werle, P. *et al.* Near-and mid-infrared laser-optical sensors for gas analysis. *Optics and lasers in engineering* **37**, 101–114 (2002).
20. Rohwedder, J. *et al.* iHWG- μ NIR: A miniaturised near-infrared gas sensor based on substrate-integrated hollow waveguides coupled to a micro-NIR-spectrophotometer. *Analyst* **139**, 3572–3576 (2014).
21. Allen, M. G. Diode laser absorption sensors for gas-dynamic and combustion flows. *Measurement Science and Technology* **9**, 545–562 (1998).
22. Harwood, M. & Jones, R. Temperature dependent ultraviolet-visible absorption cross sections of N₂O and N₂O₄: Low-temperature measurements of the equilibrium constant for 2NO₂⇌N₂O₄. *Journal of Geophysical Research: Atmospheres* **99**, 22955–22964 (1994).
23. Josowicz, M., Janata, J., Ashley, K. & Pons, S. Electrochemical and ultraviolet-visible spectroelectrochemical investigation of selectivity of potentiometric gas sensors based on polypyrrole. *Analytical Chemistry* **59**, 253–258 (1987).
24. Potyrailo, R. A., Hobbs, S. E. & Hieftje, G. M. Near-ultraviolet evanescent-wave absorption sensor based on a multimode optical fiber. *Analytical Chemistry* **70**, 1639–1645 (1998).
25. Song, J. *et al.* Electrical tracing-assisted dual-microring label-free optical bio/chemical sensors. *Optics Express* **20**, 4189–4197 (2012).
26. Schweinsberg, A. *et al.* An environmental sensor based on an integrated optical whispering gallery mode disk resonator. *Sensors and Actuators B: Chemical* **123**, 727–732 (2007).
27. Tschmelak, J., Proll, G. & Gauglitz, G. Optical biosensor for pharmaceuticals, antibiotics, hormones, endocrine disrupting chemicals and pesticides in water: Assay optimization process for estrone as example. *Talanta* **65**, 313–323 (2005).
28. Little, B. E., Chu, S. T., Haus, H. A., Foresi, J. & Laine, J.-P. Microring resonator channel dropping filters. *Journal of Lightwave Technology* **15**, 998–1005 (1997).
29. Chen, Y., Fegadolli, W. S., Jones, W. M., Scherer, A. & Li, M. Ultrasensitive gas-phase chemical sensing based on functionalized photonic crystal nanobeam cavities. *ACS Nano* **8**, 522–527 (2013).
30. Passaro, V. M., Troia, B., La Notte, M. & De Leonardis, F. Photonic resonant microcavities for chemical and biochemical sensing. *RSC Advances* **3**, 25–44 (2013).
31. Saari, L. & Seitz, W. Immobilized calcein for metal ion preconcentration. *Analytical Chemistry* **56**, 810–813 (1984).
32. Lin, X. *et al.* Pre-concentration and energy transfer enable the efficient luminescence sensing of transition metal ions by metal-organic frameworks. *Chemical Communications* **51**, 16996–16999 (2015).
33. Ni, Z., Jerrell, J. P., Cadwallader, K. R. & Masel, R. I. Metal-organic frameworks as adsorbents for trapping and preconcentration of organic phosphonates. *Analytical Chemistry* **79**, 1290–1293 (2007).
34. Zacher, D., Shekhah, O., Wöll, C. & Fischer, R. A. Thin films of metal-organic frameworks. *Chemical Society Reviews* **38**, 1418–1429 (2009).
35. Gu, Z.-Y., Wang, G. & Yan, X.-P. MOF-5 metal-organic framework as sorbent for in-field sampling and preconcentration in combination with thermal desorption GC/MS for determination of atmospheric formaldehyde. *Analytical Chemistry* **82**, 1365–1370 (2010).
36. Falcaro, P. *et al.* MOF positioning technology and device fabrication. *Chemical Society Reviews* **43**, 5513–5560 (2014).
37. Shekhah, O., Liu, J., Fischer, R. & Wöll, C. MOF thin films: Existing and future applications. *Chemical Society Reviews* **40**, 1081–1106 (2011).
38. Stavila, V., Talin, A. & Allendorf, M. MOF-based electronic and opto-electronic devices. *Chemical Society Reviews* **43**, 5994–6010 (2014).
39. Kreno, L. E. *et al.* Metal-organic framework materials as chemical sensors. *Chemical Reviews* **112**, 1105–1125 (2011).
40. Czaja, A. U., Trukhan, N. & Müller, U. Industrial applications of metal-organic frameworks. *Chemical Society Reviews* **38**, 1284–1293 (2009).
41. Seoane, B., Castellanos, S., Dikhtiarenko, A., Kapteijn, F. & Gascon, J. Multi-scale crystal engineering of metal organic frameworks. *Coordination Chemistry Reviews* **307**, 147–187 (2016).
42. Li, J.-R., Kuppler, R. J. & Zhou, H.-C. Selective gas adsorption and separation in metal-organic frameworks. *Chemical Society Reviews* **38**, 1477–1504 (2009).
43. Park, K. S. *et al.* Exceptional chemical and thermal stability of zeolitic imidazolate frameworks. *Proceedings of the National Academy of Sciences* **103**, 10186–10191 (2006).
44. Lu, G., Farha, O. K., Zhang, W., Huo, F. & Hupp, J. T. Engineering ZIF-8 thin films for hybrid MOF-based devices. *Advanced Materials* **24**, 3970–3974 (2012).
45. Cychosz, K. A., Guillet-Nicolas, R., Garcia-Martinez, J. & Thommes, M. Recent advances in the textural characterization of hierarchically structured nanoporous materials. *Chemical Society Reviews*, doi: 10.1039/C6CS00391E (2017).
46. Zhang, K. *et al.* Alcohol and water adsorption in zeolitic imidazolate frameworks. *Chemical Communications* **49**, 3245–3247 (2013).
47. Lu, G. & Hupp, J. T. Metal-organic frameworks as sensors: A ZIF-8 based fabry-pérot device as a selective sensor for chemical vapors and gases. *Journal of the American Chemical Society* **132**, 7832–7833 (2010).

48. Skoulidas, A. I. & Sholl, D. S. Self-diffusion and transport diffusion of light gases in metal-organic framework materials assessed using molecular dynamics simulations. *The Journal of Physical Chemistry B* **109**, 15760–15768 (2005).
49. Skoulidas, A. I. Molecular dynamics simulations of gas diffusion in metal-organic frameworks: Argon in CuBTC. *Journal of the American Chemical Society* **126**, 1356–1357 (2004).
50. Owens, J. C. Optical refractive index of air: Dependence on pressure, temperature and composition. *Applied Optics* **6**, 51–59 (1967).
51. Tu, M., Wannapaiboon, S., Khaletskaia, K. & Fischer, R. A. Engineering zeolitic-imidazolate framework (ZIF) thin film devices for selective detection of volatile organic compounds. *Advanced Functional Materials* **25**, 4470–4479 (2015).
52. Robinson, J. T., Chen, L. & Lipson, M. On-chip gas detection in silicon optical microcavities. *Optics Express* **16**, 4296–4301 (2008).
53. Truax, S. B. *et al.* Mass-sensitive detection of gas-phase volatile organics using disk microresonators. *Analytical Chemistry* **83**, 3305–3311 (2011).
54. Lü, Y. *et al.* MOF-templated synthesis of porous Co₃O₄ concave nanocubes with high specific surface area and their gas sensing properties. *ACS applied materials & interfaces* **6**, 4186–4195 (2014).

Acknowledgements

This work is financially supported by the Institute of Microelectronics core funding.

Author Contributions

J.F. and X.R. designed this device. T.S. and H.C. fabricated the samples. Y.X., T.L., D.L., performed the experiments. Y.G. and D.Z. supervised the project. L.L., and all other authors analysed the experimental data and edited the manuscript.

Additional Information

Competing financial interests: The authors declare no competing financial interests.

How to cite this article: Tao, J. *et al.* Hybrid Photonic Cavity with Metal-Organic Framework Coatings for the Ultra-Sensitive Detection of Volatile Organic Compounds with High Immunity to Humidity. *Sci. Rep.* **7**, 41640; doi: 10.1038/srep41640 (2017).

Publisher's note: Springer Nature remains neutral with regard to jurisdictional claims in published maps and institutional affiliations.



This work is licensed under a Creative Commons Attribution 4.0 International License. The images or other third party material in this article are included in the article's Creative Commons license, unless indicated otherwise in the credit line; if the material is not included under the Creative Commons license, users will need to obtain permission from the license holder to reproduce the material. To view a copy of this license, visit <http://creativecommons.org/licenses/by/4.0/>

© The Author(s) 2017